Computers and Fluids 271 (2024) 106165

Contents lists available at ScienceDirect

Computers and Fluids

journal homepage: www.elsevier.com/locate/compfluid

Flux vector splitting schemes applied to a conservative 1D blood flow model with transport for arteries and veins

Alessandra Spilimbergo [a,*], Eleuterio F. Toro [b], Annunziato Siviglia [b], Lucas O. Müller [a]

[a] Department of Mathematics, University of Trento, 38123 Povo, Trento, Italy
[b] Laboratory of Applied Mathematics, DICAM, University of Trento, 38123 Mesiano, Trento, Italy

ARTICLE INFO

Keywords:
Blood flow
Hyperbolic equations
Finite volume method
TV splitting

ABSTRACT

We present novel flux splitting-based numerical schemes for the 1D blood flow equations with an advection equation for a passive scalar, considering tube laws that allow to model blood flow in arteries and veins. Our schemes are inspired by the original flux vector splitting approach of Toro and Vázquez-Cendón (2012) and represent an extension of the work proposed by Toro et al. (2024), which addressed tube laws suitable for describing blood flow in arteries. Our schemes separate advection terms and pressure terms, generating two different systems of PDEs: the advection system and the pressure system, both of which have a very simple eigenstructure compared to that of the full system. We propose discretization schemes of the Godunov type that are simple and efficient. These qualities are evaluated on a suite of test problems with exact solution. A detailed efficiency analysis is performed in order to illustrate situations in which the proposed methodology results advantageous with respect to standard approaches.

1. Introduction

Blood flow models have a broad scope of applications, including the examination of healthy and diseased blood vessels hemodynamics, the development and assessment of medical devices, and the prediction of surgical outcomes. To investigate blood flow in a particular area of the cardiovascular system, the 3D incompressible Navier–Stokes equations are frequently employed as a preferred approach. The primary objective of these models is to enhance our comprehension of the intricate phenomena that occur within the cardiovascular system. It is imperative to take into account the mechanical reaction of vessel or organ walls when simulating the cardiovascular system. As a result, a fluid–structure interaction (FSI) solver is frequently created by combining a fluid model with a solid mechanics model [1,2]. However, these models can be computationally expensive, and in certain situations, it may be preferable to employ simplified 1D models derived from the 3D system.

This paper focuses on the development of novel algorithms for solving one-dimensional (1D) blood flow models [3], which have been widely employed in previous studies to satisfactorily investigate wave propagation phenomena in arteries [4–6]. More recently, their use has been extended to the highly deformable, i.e., highly non-linear, veins [7,8]. It is worth mentioning that the effectiveness of 1D blood flow models for various applications has been verified through in-silico analysis, where the predictions of these models were compared with those of more complex models [9–11], in-vitro by assessing 1D blood flow model output with respect to highly controlled experiments [12, 13] and in-vivo by assessing the capacity of these models to reproduce pressure and flow waveforms observed in the clinical context [14,15]. Moreover, when combined with zero-dimensional models, 1D blood flow models have enabled the development of comprehensive models of the entire human circulation [7,16–18]. Additionally, 1D models have proven to be valuable in their ability to be coupled with three-dimensional models, thereby providing realistic boundary conditions necessary for the analysis of detailed 3D problems that focus on the investigation of spatially localized pathological conditions [19–21].

1D blood flow models can be classified as either hyperbolic systems of balance laws or systems of partial differential equations with a dominant hyperbolic behavior, from a mathematical perspective. The specific mathematical problem to be addressed in practice will heavily rely on the chosen relationship between vessel deformation and internal blood pressure, commonly referred to as the tube law. Over the course of several decades, the employed techniques have undergone significant advancements in response to the development of numerical methods

* Corresponding author.
E-mail addresses: a.spilimbergo@unitn.it (A. Spilimbergo), eleuterio.toro@unitn.it (E.F. Toro), annunziato.siviglia@unitn.it (A. Siviglia), lucas.muller@unitn.it (L.O. Müller).

https://doi.org/10.1016/j.compfluid.2023.106165
Received 6 July 2023; Received in revised form 21 November 2023; Accepted 23 December 2023
Available online 26 December 2023
0045-7930/© 2023 The Authors. Published by Elsevier Ltd. This is an open access article under the CC BY-NC-ND license (http://creativecommons.org/licenses/by-nc-nd/4.0/).

for hyperbolic or hyperbolic-dominant partial differential equations. Among the various methods utilized, classical finite difference methods such as the Lax–Wendroff and MacCormack methods [16,22] have been employed; first- and high-order finite volume methods [23] as well as discontinuous Galerkin and Taylor–Galerkin methods [24] have also been utilized and it is worth noting the study of numerical methods with a focus on developing discretization techniques that maintain specific steady state solutions, even if this latter task can prove to be especially difficult when dealing with tubes that have varying mechanical and geometrical properties. Interested readers can refer to the introductions of [25,26] for a concise overview of this topic. One alternative approach involves employing splitting techniques that partition the initial system into two subsystems with a simpler eigenstructure compared to the entire system [27–31]. In the present study, our attention is focused on this just mentioned approach.

Our analysis involves a two-step framework that includes flux splitting at the level of partial differential equations (PDEs) and numerical methods for discretizing the ensuing problems. We build upon the flux vector splitting approach of Toro and Vázquez-Cendón [31], hereafter called the TV splitting, originally developed for the conservative Euler equations of compressible gas dynamics. In this approach the flux vector is split into advection and pressure terms: in this way, two systems of partial differential equations are obtained, one advection system and one pressure system. In Toro et al. [32] two main modifications are introduced with respect to the approach presented in [31]. The first change is at PDEs level and regards the flux of the continuity equation: in the TV splitting approach this flux is assigned to the advection system, here it is assigned to the pressure system. This property is consistent with zero-dimensional models that are based on neglecting the inertial term in the momentum equation, followed by spatial integration [32]. Furthermore, straightforward calculations show that applying the splitting methodology as presented in [31] to the 1D blood flow equations, leads to a loss of hyperbolicity of the two resulting subsystems of PDEs. The second modification is at numerical level: the numerical fluxes for the advection and the pressure systems are obtained from exact or approximate Riemann problem solvers for each system, being the Riemann problem a special Cauchy problem [33–35]. The difference concerns the way the solution of the cited Riemann solvers is used to construct the advection numerical flux. An advection equation for the concentration of a passive scalar is added, at PDEs level its conservative flux is assigned to the advection system for simplicity. In this study we extend the work of Toro et al. [32], which considered a simplified tube law usually used to describe blood flow in arteries, taking into account a more general tube law that can accurately describe blood flow in veins [23,36] (for tube laws in arteries please see [4]). The change from the simplified to the more general tube law has a significant impact on the complexity of the various elements that characterize the underlying hyperbolic PDE system: in fact, in this case, no closed form for the generalized Riemann invariants is available, affecting the efficiency of the two-rarefaction approximate Riemann solver proposed in [32]. We first extend the forementioned solver to this more general setting and then propose a linearized solution of it. We then use a set of problems to test their robustness and accuracy: for these tests these schemes are simple, robust, and accurate compared to existing methods, and correctly solve the contact waves. Finally, an efficiency test is performed.

Noteworthy, adopting the TV splitting approach has several properties of potential interest for blood flow simulations in complex vessel networks. Separating the original problem into an advection and a pressure system simplifies the wave relations that need to be enforced when a two-rarefaction Riemann solver is adopted. For more general blood flow models, wave relations can be very complex and require to solve non-linear ordinary differential equations to be evaluated (see [37] for more details). Having simplified wave relations will also have a positive impact not only in the numerical method used to solve the blood flow equations within vessels, but also in the determination of coupling conditions between one-dimensional domains, which in turn are determined by wave relations [4,5].

The manuscript is organized as follows: we start with a brief review of the 1D blood flow equations with an advection equation for the passive scalar and their exact solution of the Riemann problem (Section 2), in Section 3 we describe the proposed flux splitting at the level of the PDEs, in Section 4 we briefly review some theoretical aspects of the Riemann problem for the pressure system, and in Section 5 we present the two approximate Riemann solvers for the pressure system mentioned above. Finally, the numerical flux splitting scheme is presented in Section 6, the numerical results are given in Section 7, while in Section 7.2 the efficiency analysis is performed. The conclusions are drawn in Section 8.

2. 1D blood flow model with transport

2.1. Governing equations

Assuming a deformable axially symmetric vessel configuration in three space dimensions at time t, and assuming one-dimensional flow in the axial direction x, the 1D blood flow model with continuous mechanical and geometrical properties reads

$$\begin{cases} \partial_t A + \partial_x(Au) = 0, \\ \partial_t(Au) + \partial_x(Au^2) + \frac{A}{\rho}\partial_x p = 0, \\ \partial_t(A\phi) + \partial_x(Au\phi) = 0, \end{cases} \tag{1}$$

where $A(x,t)$ is the cross-sectional area of the vessel at position x and time t, with the assumption that $A \in \mathbb{R}^+$. $u(x,t)$ is the averaged velocity of blood at a cross section, $p(x,t)$ is the pressure, ρ is the density of blood, assumed constant, $\phi(x,t) \in \mathbb{R}_0^+$ is the concentration of the passive scalar. The first and second equations in (1) represent the conservation of mass and momentum, while the third concerns the advection equation for the passive scalar ϕ. To close the system we adopt the following tube law

$$p = p_e + \psi(A, K, A_0), \tag{2}$$

where p_e is the external pressure, $\psi(A, K, A_0)$ is the *transmural pressure*, assumed of the form

$$\psi(A, K, A_0) = K\left[\left(\frac{A}{A_0}\right)^m - \left(\frac{A}{A_0}\right)^n\right], \tag{3}$$

with

$$K = \begin{cases} \dfrac{E}{(1-\nu^2)}\left(\dfrac{h_0}{R_0}\right) & \text{for arteries,} \\ \dfrac{E}{12(1-\nu^2)}\left(\dfrac{h_0}{R_0}\right)^3 & \text{for veins,} \end{cases} \tag{4}$$

$$m = \begin{cases} 1/2 & \text{for arteries,} \\ 10 & \text{for veins,} \end{cases} \qquad n = \begin{cases} 0 & \text{for arteries,} \\ -3/2 & \text{for veins.} \end{cases} \tag{5}$$

Here h_0 is the wall thickness of the vessel; A_0 and R_0 are the cross-sectional area of the vessel and the radius at equilibrium: $\psi(A, K, A_0) = 0$; E is the Young's modulus; ν is the Poisson's ratio, which is taken as $\nu = \frac{1}{2}$, m and n are real numbers and are generally taken as $m > 0$ and $-2 \le n \le 0$. $K \in \mathbb{R}^+$, $A_0 \in \mathbb{R}^+$, $R_0 \in \mathbb{R}^+$, $p_e \in \mathbb{R}$, $h_0 \in \mathbb{R}^+$, $E \in \mathbb{R}^+$ are constants.

System (1) is conservative, in fact it can be written as

$$\begin{cases} \partial_t A + \partial_x(Au) = 0, \\ \partial_t(Au) + \partial_x\left(Au^2 + \int c(A)^2 dA\right) = 0, \\ \partial_t(A\phi) + \partial_x(Au\phi) = 0, \end{cases} \tag{6}$$

i.e. in the form

$$\partial_t \mathbf{Q} + \partial_x \mathbf{F}(\mathbf{Q}) = 0, \tag{7}$$

with

$$\mathbf{Q} = \begin{bmatrix} A \\ Au \\ A\phi \end{bmatrix},$$

$$\mathbf{F}(\mathbf{Q}) = \begin{bmatrix} Au \\ Au^2 + \int c(A)^2\, dA \\ Au\phi \end{bmatrix} = \begin{bmatrix} Au \\ Au^2 + \frac{KA}{\rho}\left(\frac{m}{m+1}\left(\frac{A}{A_0}\right)^m - \frac{n}{n+1}\left(\frac{A}{A_0}\right)^n\right) \\ Au\phi \end{bmatrix}, \tag{8}$$

where

$$c(A) = \sqrt{\frac{A}{\rho}\frac{\partial p}{\partial A}} = \sqrt{\frac{K}{\rho}\left[m\left(\frac{A}{A_0}\right)^m - n\left(\frac{A}{A_0}\right)^n\right]}, \tag{9}$$

is the *wave speed* which is always real, for the choice of m and n in (5) [38].

The Jacobian of system (6) is

$$\mathcal{J}(\mathbf{Q}) = \begin{bmatrix} 0 & 1 & 0 \\ c^2 - u^2 & 2u & 0 \\ -u\phi & \phi & u \end{bmatrix}, \tag{10}$$

and its eigenvalues are given by

$$\lambda_1 = u - c, \qquad \lambda_2 = u, \qquad \lambda_3 = u + c\,. \tag{11}$$

A possible choice of right eigenvectors corresponding to eigenvalues (11) is

$$\mathbf{R}_1 = \begin{bmatrix} 1 \\ u - c \\ \phi \end{bmatrix}, \qquad \mathbf{R}_2 = \begin{bmatrix} 0 \\ 0 \\ 1 \end{bmatrix}, \qquad \mathbf{R}_3 = \begin{bmatrix} 1 \\ u + c \\ \phi \end{bmatrix}. \tag{12}$$

Remark 2.1. Note that in this article we refer to the flow rate as Au or $q = Au$, and also refer to c in (9) in this way: for example, we write c_L for $c(A_L)$, c_R for $c(A_R)$, c^* for $c(A^*)$, and so on.

Proposition 2.1 (*Hyperbolicity*)**.** *The system of conservation laws defined in (1) is strictly hyperbolic under the following hypotheses:*

1. *the set of admissible solutions is restricted to* $\mathbf{Q} \in \Omega = [\mathbb{R}^+ \times \mathbb{R} \times \mathbb{R}_0^+] \subset \mathbb{R}^3$*;*
2. *the tube law is a monotonically increasing function of the cross-sectional area A, i.e.* $\frac{\partial p}{\partial A} > 0$.

Proof. It is straightforward to prove that under the specified hypotheses, eigenvalues (11) will always be real and distinct $\forall \mathbf{Q} \in \Omega$. In particular hypothesis 2 is satisfied by the parameters given in (4), (5).

Proposition 2.2 (*Nature of the λ_1- and λ_3-Characteristic Fields*)**.** *Under the hypotheses of Proposition 2.1 and under the restrictions on coefficients m and n specified in (5), the λ_1- and λ_3-characteristic fields are genuinely non-linear with*

$$\begin{aligned} &\nabla\lambda_1(\mathbf{Q}) \cdot \mathbf{R}_1(\mathbf{Q}) < 0, \quad \forall \mathbf{Q} \in \Omega, \\ &\nabla\lambda_3(\mathbf{Q}) \cdot \mathbf{R}_3(\mathbf{Q}) > 0, \quad \forall \mathbf{Q} \in \Omega. \end{aligned} \tag{13}$$

Proof. Please see Toro and Siviglia [38].

Proposition 2.3 (*Nature of the λ_2-Characteristic Field*)**.** *Under the hypotheses of Proposition 2.1, the λ_2-characteristic field is linearly degenerate.*

Proof. It is straightforward to show that

$$\nabla\lambda_2(\mathbf{Q}) \cdot \mathbf{R}_2(\mathbf{Q}) = 0, \quad \forall \mathbf{Q} \in \Omega. \tag{14}$$

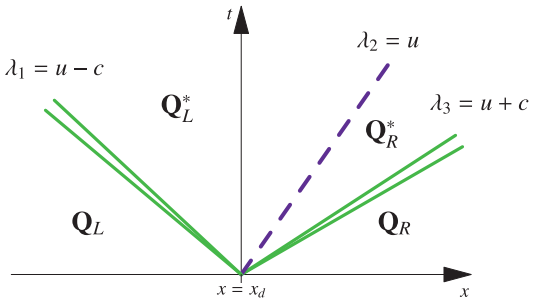

Fig. 1. A possible configuration of the exact solution of the Riemann problem (18). The green solid lines represent waves associated with genuinely non-linear fields, that can be either shocks or rarefactions. The purple dashed line represents the contact discontinuity for the passive scalar and is associated with a linearly degenerate field. The λ_1-wave is sometimes called left wave, while the λ_3- one, right wave. It follows that the related wave patterns in this paper will be called *left rarefaction/left shock* or *right rarefaction/right shock*.

Proposition 2.4 (*Generalized Riemann Invariants for the λ_1- and λ_3-Characteristic Fields*)**.** *The Riemann invariants are given by*

$$u + \int \frac{c(A)}{A} dA = const, \quad \phi = const, \tag{15}$$

for the λ_1-characteristic field,

$$u - \int \frac{c(A)}{A} dA = const, \quad \phi = const, \tag{16}$$

for the λ_3-characteristic field.

Proof. Omitted. See Toro and Siviglia [38].

Proposition 2.5 (*Generalized Riemann Invariants for the λ_2-Characteristic Field*)**.** *The generalized Riemann invariants for the λ_2-characteristic field are*

$$A = const, \quad q = const, \quad \phi \neq const. \tag{17}$$

Proof. Omitted. See Toro and Siviglia [38].

2.2. Riemann problem for the full system

The Riemann problem for system (7) is

$$\begin{cases} \partial_t \mathbf{Q} + \partial_x \mathbf{F}(\mathbf{Q}) = 0, & x \in \mathbb{R}, \quad t > 0, \\ \mathbf{Q}(x,0) = \begin{cases} \mathbf{Q}_L & \text{if} \quad x < x_d, \\ \mathbf{Q}_R & \text{if} \quad x > x_d, \end{cases} \end{cases} \tag{18}$$

where $x_d \in \mathbb{R}$ is the spatial location of the discontinuity at $t = 0$. The left and right initial conditions are $\mathbf{Q}_L$ and $\mathbf{Q}_R$, while the unknowns are

$$\mathbf{Q}_L^* = \begin{bmatrix} A^* \\ A^*u^* \\ A^*\phi_L^* \end{bmatrix}, \quad \mathbf{Q}_R^* = \begin{bmatrix} A^* \\ A^*u^* \\ A^*\phi_R^* \end{bmatrix}. \tag{19}$$

Fig. 1 depicts the structure of the exact solution of the Riemann problem (18). The waves associated with the genuinely non-linear λ_1- and λ_3-characteristic fields can be either shocks (elastic jumps) or rarefactions [39], while the wave related to the linearly degenerate λ_2-characteristic field is a contact discontinuity.

The complete exact solution of the Riemann problem for the entire system is not explicitly provided in this paper, as it is widely documented in existing literature. For comprehensive details, we refer interested readers to sources such as Toro and Siviglia [38] and Spilimbergo et al. [40]. It is important to note that the exact solution of the Riemann problem for the 1D blood flow equations with continuous parameters, which we consider in this study, is a specific case within

the broader exact solution framework discussed in Toro and Siviglia [38],Spilimbergo et al. [40] for the 1D blood flow equations with discontinuous parameters.

3. Flux splitting at the level of PDEs

We split $\mathbf{F}(\mathbf{Q})$ in (8) into advection and pressure fluxes as follows

$$\mathbf{F}(\mathbf{Q}) = \boldsymbol{\mathcal{A}}(\mathbf{Q}) + \boldsymbol{\mathcal{P}}(\mathbf{Q}), \tag{20}$$

and we propose to split system (7) via (20) into the two subsystems

$$\begin{cases} \partial_t \mathbf{Q} + \partial_x \boldsymbol{\mathcal{A}}(\mathbf{Q}) = 0, & \text{(21a)} \\ \partial_t \mathbf{Q} + \partial_x \boldsymbol{\mathcal{P}}(\mathbf{Q}) = 0, & \text{(21b)} \end{cases}$$

where

$$\mathbf{Q} = \begin{bmatrix} A \\ Au \\ A\phi \end{bmatrix}, \quad \boldsymbol{\mathcal{A}}(\mathbf{Q}) = \begin{bmatrix} 0 \\ Au^2 \\ Au\phi \end{bmatrix},$$
$$\boldsymbol{\mathcal{P}}(\mathbf{Q}) = \begin{bmatrix} Au \\ \int c(A)^2\, dA \\ 0 \end{bmatrix} = \begin{bmatrix} Au \\ \frac{KA}{\rho}\left(\frac{m}{m+1}\left(\frac{A}{A_0}\right)^m - \frac{n}{n+1}\left(\frac{A}{A_0}\right)^n\right) \\ 0 \end{bmatrix}. \tag{22}$$

System (21a) is called "advection system", system (21b) is called "pressure system". As it will be presented in Section 6, the aim is to compute a numerical flux

$$\mathbf{F}_{i+\frac{1}{2}} = \boldsymbol{\mathcal{A}}_{i+\frac{1}{2}} + \boldsymbol{\mathcal{P}}_{i+\frac{1}{2}}, \tag{23}$$

where $\boldsymbol{\mathcal{A}}_{i+\frac{1}{2}}$ and $\boldsymbol{\mathcal{P}}_{i+\frac{1}{2}}$ are obtained from appropriate Cauchy problems for the advection (21a) and pressure (21b) systems, respectively. The numerical strategy to determine the advection and pressure numerical fluxes in (23) relies on first solving the Riemann problem for the pressure system in (21b). The solution of this system will fully determine the pressure numerical flux $\boldsymbol{\mathcal{P}}_{i+\frac{1}{2}}$ and will also provide advection information for determining the advection numerical flux $\boldsymbol{\mathcal{A}}_{i+\frac{1}{2}}$ in (23). In other words, we only need to solve the Riemann problem for the pressure system in (21b). This is carried out in the next sections.

4. Riemann problem for the pressure system

The Jacobian of system (21b) is

$$\boldsymbol{\mathcal{J}}_{\mathcal{P}}(\mathbf{Q}) = \begin{bmatrix} 0 & 1 & 0 \\ c^2 & 0 & 0 \\ 0 & 0 & 0 \end{bmatrix}. \tag{24}$$

The eigenvalues of $\boldsymbol{\mathcal{J}}_{\mathcal{P}}(\mathbf{Q})$ are given by

$$\lambda_{\mathcal{P}1} = -c, \qquad \lambda_{\mathcal{P}2} = 0, \qquad \lambda_{\mathcal{P}3} = c, \tag{25}$$

moreover a possible choice of right eigenvectors corresponding to eigenvalues (25) is

$$\mathbf{R}_{\mathcal{P}1} = \begin{bmatrix} 1 \\ -c \\ 0 \end{bmatrix}, \qquad \mathbf{R}_{\mathcal{P}2} = \begin{bmatrix} 0 \\ 0 \\ 1 \end{bmatrix}, \qquad \mathbf{R}_{\mathcal{P}3} = \begin{bmatrix} 1 \\ c \\ 0 \end{bmatrix}. \tag{26}$$

where c is the wave speed (9).

We can now state the following propositions about the eigenstructure of pressure system (21b).

Proposition 4.1 (*Hyperbolicity*). *System (21b) is strictly hyperbolic under the following hypotheses:*

1. *the set of admissible solutions is restricted to* $\mathbf{Q} \in \Omega = [\mathbb{R}^+ \times \mathbb{R} \times \mathbb{R}_0^+] \subset \mathbb{R}^3$;
2. *the tube law is a monotonically increasing function of the cross-sectional area A, i.e.* $\frac{\partial p}{\partial A} > 0$.

Proof. This can be clearly seen from the definition of wave speed given in (9). Under the conditions considered in this proposition $c \in \mathbb{R}^+ \ \forall \mathbf{Q} \in \Omega$, which results in $\lambda_{\mathcal{P}1} \in \mathbb{R}^-$, $\lambda_{\mathcal{P}3} \in \mathbb{R}^+$, $\forall \mathbf{Q} \in \Omega$. In particular this is true for the parameters given in (4), (5).

Proposition 4.2 (*Nature of the $\lambda_{\mathcal{P}1}$- and $\lambda_{\mathcal{P}3}$-Characteristic Fields*). *Under the hypotheses of Proposition 4.1, in case of arteries (parameters are given in (4),(5)) the $\lambda_{\mathcal{P}1}$- and $\lambda_{\mathcal{P}3}$-characteristic fields are genuinely non-linear with*

$$\begin{aligned} &\nabla\lambda_{\mathcal{P}1}(\mathbf{Q}) \cdot \mathbf{R}_{\mathcal{P}1}(\mathbf{Q}) < 0, \quad \forall \mathbf{Q} \in \Omega, \\ &\nabla\lambda_{\mathcal{P}3}(\mathbf{Q}) \cdot \mathbf{R}_{\mathcal{P}3}(\mathbf{Q}) > 0, \quad \forall \mathbf{Q} \in \Omega, \end{aligned} \tag{27}$$

instead in case of veins, they are not. In fact

$$\begin{aligned} \nabla\lambda_{\mathcal{P}1}(\mathbf{Q}) \cdot \mathbf{R}_{\mathcal{P}1}(\mathbf{Q}) \quad &\begin{cases} > 0 & for \quad A < A_c, \\ = 0 & for \quad A = A_c, \\ < 0 & for \quad A > A_c, \end{cases} \\ \nabla\lambda_{\mathcal{P}3}(\mathbf{Q}) \cdot \mathbf{R}_{\mathcal{P}3}(\mathbf{Q}) \quad &\begin{cases} < 0 & for \quad A < A_c, \\ = 0 & for \quad A = A_c, \\ > 0 & for \quad A > A_c, \end{cases} \end{aligned} \tag{28}$$

where A_c, for parameters in (5), is

$$A_c \approx 0.7190\, A_0. \tag{29}$$

Proof. It can be easily verified that

$$\nabla\lambda_{\mathcal{P}1}(\mathbf{Q}) \cdot \mathbf{R}_{\mathcal{P}1}(\mathbf{Q}) = -\frac{\partial c}{\partial A}, \tag{30}$$

and

$$\nabla\lambda_{\mathcal{P}3}(\mathbf{Q}) \cdot \mathbf{R}_{\mathcal{P}3}(\mathbf{Q}) = \frac{\partial c}{\partial A}, \tag{31}$$

where $\mathbf{R}_{\mathcal{P}1}$ and $\mathbf{R}_{\mathcal{P}3}$ are the right eigenvectors (26). For genuine non-linearity we must prove that $\frac{\partial c}{\partial A} \neq 0$. Having

$$\frac{\partial c}{\partial A} = \frac{\frac{K}{\rho}\left(\left(\frac{A}{A_0}\right)^m m^2 - \left(\frac{A}{A_0}\right)^n n^2\right)}{2A\sqrt{\frac{K}{\rho}\left(\left(\frac{A}{A_0}\right)^m m - \left(\frac{A}{A_0}\right)^n n\right)}}, \tag{32}$$

being

$$\sqrt{\frac{K}{\rho}\left(\left(\frac{A}{A_0}\right)^m m - \left(\frac{A}{A_0}\right)^n n\right)} = c > 0, \tag{33}$$

by hypothesis, with c as in (9) and being by hypothesis $K > 0$, $\rho > 0$, $A_0 > 0$ and $A > 0$, we must prove that

$$\left(\left(\frac{A}{A_0}\right)^m m^2 - \left(\frac{A}{A_0}\right)^n n^2\right) \neq 0, \tag{34}$$

for our considered values of variables and parameters. It is easy to verify that for the case of arteries, i.e $m = 0.5$ and $n = 0$, (34) always holds, and in particular

$$\frac{\partial c}{\partial A} > 0, \quad \forall A \in \mathbb{R}^+, \tag{35}$$

that gives the result. On the contrary, for the case of veins i.e $m = 10$ and $n = -1.5$

$$y(\zeta) = \zeta^{10} 10^2 - \zeta^{-1.5} 1.5^2, \tag{36}$$

changes its sign from negative to positive and there exists one and only ζ_z in the interval $\mathcal{I} =]0, \infty[$ such that $y(\zeta_z) = 0$, that is approximately

$$\zeta_z = \frac{A_c}{A_0} \approx 0.7190, \tag{37}$$

this means that in case of veins

$$\frac{\partial c}{\partial A} \quad \begin{cases} < 0 & \text{for} \quad A < A_c, \\ = 0 & \text{for} \quad A = A_c, \\ > 0 & \text{for} \quad A > A_c. \end{cases} \tag{38}$$

Proposition 4.3 (*Nature of the $\lambda_{\mathcal{P}2}$-Characteristic Field*)**.** *Under the hypotheses of Proposition 4.1, the $\lambda_{\mathcal{P}2}$-characteristic field is linearly degenerate.*

Proof. It is straightforward to show that

$$\nabla \lambda_{\mathcal{P}2}(\mathbf{Q}) \cdot \mathbf{R}_{\mathcal{P}2}(\mathbf{Q}) = 0, \quad \forall \mathbf{Q} \in \Omega. \tag{39}$$

Proposition 4.4 (*Generalized Riemann Invariants for the $\lambda_{\mathcal{P}1}$- and $\lambda_{\mathcal{P}3}$-Characteristic Fields*)**.** *The Riemann invariants are given by*

$$q + \int c(A) dA = const, \quad A\phi = const, \tag{40}$$

for the $\lambda_{\mathcal{P}1}$-characteristic field,

$$q - \int c(A) dA = const, \quad A\phi = const, \tag{41}$$

for the $\lambda_{\mathcal{P}3}$-characteristic field.

Proof. The problem can be solved applying the generalized Riemann invariant method [38], i.e for a given hyperbolic system of n unknowns $[w_1, w_2, \dots, w_n]^T$, for any $\lambda_{\mathcal{P}k}$-characteristic field with right eigenvector $\mathbf{R}_{\mathcal{P}k} = [r_{1,k}, r_{2,k}, \dots, r_{n,k}]^T$ the generalized Riemann invariants are solutions of the following $n-1$ ordinary differential equations in phase-plane

$$\frac{dw_1}{r_{1,k}} = \frac{dw_2}{r_{2,k}} = \cdots = \frac{dw_n}{r_{n,k}}. \tag{42}$$

For the $\lambda_{\mathcal{P}1}$-characteristic field we have

$$\frac{dA}{1} = \frac{dq}{-c} = \frac{d(A\phi)}{0}, \tag{43}$$

i.e. from the first and the second term

$$(-c) dA = dq, \tag{44}$$

and from the third

$$d(A\phi) = 0 \Longrightarrow A\phi = const. \tag{45}$$

For the $\lambda_{\mathcal{P}3}$-characteristic field

$$\frac{dA}{1} = \frac{dq}{c} = \frac{d(A\phi)}{0}, \tag{46}$$

i.e. from the first and the second term

$$c\, dA = dq, \tag{47}$$

and from the third

$$d(A\phi) = 0 \Longrightarrow A\phi = const. \tag{48}$$

Proposition 4.5 (*Generalized Riemann Invariants for the $\lambda_{\mathcal{P}2}$-Characteristic Field*)**.** *The generalized Riemann invariants for the $\lambda_{\mathcal{P}2}$-characteristic field are*

$$A = const, \quad q = const, \quad \phi \neq const. \tag{49}$$

Proof. Applying again the generalized Riemann invariant method [38] for the $\lambda_{\mathcal{P}2}$-characteristic field, we obtain

$$\frac{dA}{0} = \frac{dq}{0} = \frac{d(A\phi)}{1}, \tag{50}$$

that implies

$$A = const, \qquad q = const, \qquad \phi \neq const. \tag{51}$$

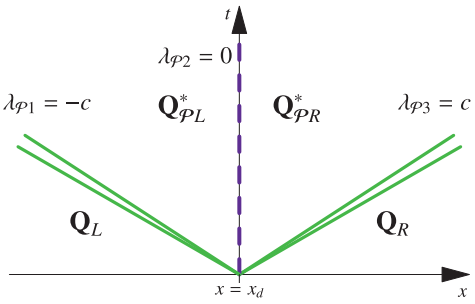

Fig. 2. The configuration of the exact solution of the Riemann problem for the pressure system (52). The green solid lines, in case of arteries, represent waves associated with genuinely non-linear fields, while in case of veins this property is lost. The purple dashed line represents the contact discontinuity for the passive scalar and is associated with a linearly degenerate field.

The Riemann problem for system (21b) is

$$\begin{cases} \partial_t \mathbf{Q} + \partial_x \boldsymbol{\mathcal{P}}(\mathbf{Q}) = 0, \quad x \in \mathbb{R}, \quad t > 0, \\ \mathbf{Q}(x,0) = \begin{cases} \mathbf{Q}_L & \text{if} \quad x < x_d, \\ \mathbf{Q}_R, & \text{if} \quad x > x_d, \end{cases} \end{cases} \tag{52}$$

where $x_d \in \mathbb{R}$ is the spatial location of the discontinuity at $t = 0$. The initial data are $\mathbf{Q}_L$ and $\mathbf{Q}_R$. The unknowns are $\mathbf{Q}^*_{\mathcal{P}L}$ and $\mathbf{Q}^*_{\mathcal{P}R}$ defined as

$$\begin{aligned} \mathbf{Q}^*_{\mathcal{P}L} &= \begin{bmatrix} A^*_L \\ q^*_L \\ (A\phi)^*_L \end{bmatrix} = \begin{bmatrix} A^* \\ q^* \\ A^*\phi^*_L \end{bmatrix} = \begin{bmatrix} A^* \\ A^*u^* \\ A^*\phi^*_L \end{bmatrix}, \\ \mathbf{Q}^*_{\mathcal{P}R} &= \begin{bmatrix} A^*_R \\ q^*_R \\ (A\phi)^*_R \end{bmatrix} = \begin{bmatrix} A^* \\ q^* \\ A^*\phi^*_R \end{bmatrix} = \begin{bmatrix} A^* \\ A^*u^* \\ A^*\phi^*_R \end{bmatrix}, \end{aligned} \tag{53}$$

thanks to Proposition 4.5 that states clearly that across the $\lambda_{\mathcal{P}2}$-wave, only variable ϕ changes. Fig. 2 depicts the structure of the exact solution of the Riemann problem (52) for the pressure system (21b): the wave related to the $\lambda_{\mathcal{P}2}$-characteristic field is associated with a linearly degenerate field and is a contact discontinuity, instead the waves related to the $\lambda_{\mathcal{P}1}$- and $\lambda_{\mathcal{P}3}$-characteristic fields, in case of arteries, are associated with genuine non-linear fields (Proposition 4.2) and can be either shocks (elastic jumps) or rarefactions [39]; in case of veins, the loss of genuine non-linearity can lead to a formation of compound waves [41].

Remark 4.1. It is worth noting that for the pressure system, the waves associated with $\lambda_{\mathcal{P}1}$- and $\lambda_{\mathcal{P}3}$-characteristic fields will always be *subsonic*, since

$$\lambda_{\mathcal{P}1}(\mathbf{Q}) < 0 \quad \text{and} \quad \lambda_{\mathcal{P}3}(\mathbf{Q}) > 0, \quad \text{i.e. } c > 0, \quad \forall \mathbf{Q} \in \Omega. \tag{54}$$

Remark 4.2. In this paper, we do not provide a complete description of the exact solution of the Riemann problem for the pressure system (52). Our approach considers a simplified configuration characterized by two rarefaction waves associated with the $\lambda_{\mathcal{P}1}$- and $\lambda_{\mathcal{P}3}$-fields, with a contact discontinuity linked to the $\lambda_{\mathcal{P}2}$-field situated between them. This choice is motivated by the proposed numerical schemes and also by the complexity of the mathematical analysis of the mentioned solution in the case of veins, due to the lack of genuine non-linearity of the $\lambda_{\mathcal{P}1}$- and $\lambda_{\mathcal{P}3}$-characteristic fields (Proposition 4.2). A complete description of the solution of the Riemann problem for tube laws with respect to veins will be treated in a separate paper. Here we restrict ourselves to observing empirically how the splitting schemes behave in cases where the loss of genuine non-linearity occurs for the $\lambda_{\mathcal{P}1}$- and $\lambda_{\mathcal{P}3}$-characteristic fields of the pressure system.

5. Approximate Riemann solvers for the pressure system

Having introduced the relations across the waves (Propositions 4.4, 4.5), we can introduce two approximate Riemann solvers for the pressure system (21b). For the purposes of this article, we restrict ourselves to the presentation of the solution in the *Star Region* (i.e., the unknowns $\mathbf{Q}^*_{\mathcal{P}L}$ and $\mathbf{Q}^*_{\mathcal{P}R}$).

5.1. A two-rarefaction approximate Riemann solver for the pressure system

The two-rarefaction approximate Riemann solver operates under the assumption of two rarefaction waves, disregarding the shock wave relations. The solution in the Star Region in this case is

$$\mathbf{Q}^*_{TR,L} = \begin{bmatrix} A^*_{TR} \\ q^*_{TR} \\ A^*_{TR}\phi^*_{TR,L} \end{bmatrix}, \quad \mathbf{Q}^*_{TR,R} = \begin{bmatrix} A^*_{TR} \\ q^*_{TR} \\ A^*_{TR}\phi^*_{TR,R} \end{bmatrix}. \tag{55}$$

Given the wave relations described in Proposition 4.4

$$\begin{aligned} q^* &= q_L - \int_{A_L}^{A^*} c(A)dA, \\ q^* &= q_R + \int_{A_R}^{A^*} c(A)dA, \end{aligned} \tag{56}$$

with c the wave speed (9), in case of left and right rarefactions

$$\begin{aligned} q^*_{TR} &= \frac{1}{2}(q_L + q_R) + \frac{1}{2}\left(\int_{A_R}^{A^*} c(A)dA - \int_{A_L}^{A^*} c(A)dA\right) \\ &= \frac{1}{2}(q_L + q_R) - \frac{1}{2}\int_{A_L}^{A_R} c(A)dA. \end{aligned} \tag{57}$$

Having found q^*_{TR}, we obtain A^*_{TR} solving one of (56), for example

$$q^*_{TR} = q_L - \int_{A_L}^{A^*_{TR}} c(A)dA, \tag{58}$$

where the integrals in case of veins are calculated with a six-point Gauss quadrature rule thanks to the Python function *scipy.integrate.fixed_quad*, and Eq. (58) is solved with a globally convergent Newton–Raphson method Appendix (for arteries with $m = 0.5$ and $n = 0$ in (5), the solution is explicit).

Regarding the last variable, considering Propositions 4.4 and 4.5

$$\phi^*_{TR,L} = \frac{A_L}{A^*_{TR}}\phi_L, \qquad \phi^*_{TR,R} = \frac{A_R}{A^*_{TR}}\phi_R. \tag{59}$$

5.2. A linearized two-rarefaction approximate Riemann solver for the pressure system

Now we proceed as in the case of the two-rarefaction Riemann solver and additionally approximate the relations (56). In this case, the solution in the *Star Region* is

$$\mathbf{Q}^*_{LTR,L} = \begin{bmatrix} A^*_{LTR} \\ q^*_{LTR} \\ A^*_{LTR}\phi^*_{LTR,L} \end{bmatrix}, \quad \mathbf{Q}^*_{LTR,R} = \begin{bmatrix} A^*_{LTR} \\ q^*_{LTR} \\ A^*_{LTR}\phi^*_{LTR,R} \end{bmatrix}. \tag{60}$$

Given the wave relations from Proposition 4.4 described in (56), we approximate the integrals in this way

$$\int_{A_L}^{A^*} c(A)dA \approx c_L(A^* - A_L), \tag{61}$$

$$\int_{A_R}^{A^*} c(A)dA \approx c_R(A^* - A_R). \tag{62}$$

Solving the system

$$\begin{cases} q^* = q_L - c_L(A^* - A_L), \\ q^* = q_R + c_R(A^* - A_R), \end{cases} \tag{63}$$

we obtain

$$\begin{aligned} q^*_{LTR} &= \frac{c_R(A_L c_L - A_R c_L + q_L) + c_L q_R}{c_L + c_R}, \\ A^*_{LTR} &= \frac{A_L c_L + A_R c_R + q_L - q_R}{c_L + c_R}. \end{aligned} \tag{64}$$

For the definition of c_L and c_R we refer again to Remark 2.1.

Regarding the last variable, as before

$$\phi^*_{LTR,L} = \frac{A_L}{A^*_{LTR}}\phi_L, \qquad \phi^*_{LTR,R} = \frac{A_R}{A^*_{LTR}}\phi_R. \tag{65}$$

6. Advection-pressure numerical splitting schemes for the complete system of 1D blood flow equations with transport

To numerically solve the system (1), we employ a conservative method following the approach outlined in Toro and Vázquez-Cendón [31]. The numerical scheme is

$$\mathbf{Q}_i^{n+1} = \mathbf{Q}_i^n - \frac{\Delta t}{\Delta x}(\mathbf{F}_{i+\frac{1}{2}} - \mathbf{F}_{i-\frac{1}{2}}), \tag{66}$$

where

$$\mathbf{Q}_i^n \approx \frac{1}{\Delta x}\int_{x_{i-\frac{1}{2}}}^{x_{i+\frac{1}{2}}} \mathbf{Q}(x, t^n)dx, \tag{67}$$

with $\Delta x = x_{i+\frac{1}{2}} - x_{i-\frac{1}{2}}$, $\Delta t = t^{n+1} - t^n$. As anticipated in Section 3, the aim is to compute a numerical flux

$$\mathbf{F}_{i+\frac{1}{2}} = \boldsymbol{\mathcal{A}}_{i+\frac{1}{2}} + \boldsymbol{\mathcal{P}}_{i+\frac{1}{2}}, \tag{68}$$

where $\boldsymbol{\mathcal{A}}_{i+\frac{1}{2}}$ and $\boldsymbol{\mathcal{P}}_{i+\frac{1}{2}}$ are obtained from appropriate Cauchy problems for the advection (21a) and pressure (21b) systems, respectively.

We define

$$\boldsymbol{\mathcal{P}}_{i+\frac{1}{2}} = \boldsymbol{\mathcal{P}}(\mathbf{Q}_{i+\frac{1}{2}}(0)), \tag{69}$$

where $\boldsymbol{\mathcal{P}}$ is in (22) and $\mathbf{Q}_{i+\frac{1}{2}}(0)$ denotes the Godunov state, i.e. the value $\mathbf{Q}_{i+\frac{1}{2}}\left(\frac{x - x_{i+\frac{1}{2}}}{t}\right)$ calculated at $\frac{x - x_{i+\frac{1}{2}}}{t} = 0$, i.e. the solution of the following Riemann problem

$$\begin{cases} \partial_t \mathbf{Q} + \partial_x \boldsymbol{\mathcal{P}}(\mathbf{Q}) = 0, \quad x \in \mathbb{R}, \quad t > t^n, \\ \mathbf{Q}(x, t^n) = \begin{cases} \mathbf{Q}_L = \mathbf{Q}_i^n, & \text{if} \quad x < x_{i+\frac{1}{2}}, \\ \mathbf{Q}_R = \mathbf{Q}_{i+1}^n, & \text{if} \quad x > x_{i+\frac{1}{2}}, \end{cases} \end{cases} \tag{70}$$

evaluated at the interface $x_{i+\frac{1}{2}}$, for each cell i. Due to the fact that the wave configuration of the solution of the Riemann problem for the pressure system (70) will always result in two subsonic waves, $\mathbf{Q}_{i+\frac{1}{2}}(0) = \mathbf{Q}^*_{\text{PRESS},i+\frac{1}{2}} = [A^*_{\text{PRESS},i+\frac{1}{2}}, q^*_{\text{PRESS},i+\frac{1}{2}}, A^*_{\text{PRESS},i+\frac{1}{2}}\phi^*_{\text{PRESS},i+\frac{1}{2}}]^T$, the solution in the Star Region of the Riemann problem (70) for each cell i.

$\boldsymbol{\mathcal{A}}_{i+\frac{1}{2}}$ is computed as proposed in Toro et al. [42], which represents a modification of the original splitting presented in Toro and Vázquez-Cendón [31] namely,

$$\boldsymbol{\mathcal{A}}_{i+\frac{1}{2}} = \begin{bmatrix} 0 \\ q^*_{\text{PRESS},i+\frac{1}{2}} u_k \\ q^*_{\text{PRESS},i+\frac{1}{2}} \phi_k \end{bmatrix}, \tag{71}$$

where

$$u_k = \begin{cases} u_L & \text{if} \quad q^*_{\text{PRESS},i+\frac{1}{2}} > 0, \\ u_R & \text{if} \quad q^*_{\text{PRESS},i+\frac{1}{2}} \le 0, \end{cases} \qquad \phi_k = \begin{cases} \phi_L & \text{if} \quad q^*_{\text{PRESS},i+\frac{1}{2}} > 0, \\ \phi_R & \text{if} \quad q^*_{\text{PRESS},i+\frac{1}{2}} \le 0. \end{cases} \tag{72}$$

To compute $\mathbf{Q}^*_{\text{PRESS},i+\frac{1}{2}}$ we use two different methods

Table 1
Initial conditions for Tests from 1 to 6. The wave patterns are: R=rarefaction, C=contact discontinuity, S=shock. The units of measures used for this paper are: m, s, Kg, Pa.

Test	A_L[m^2]	u_L[m/s]	ϕ_L	A_R[m^2]	u_R[m/s]	ϕ_R	Wave pattern
1	$3.50 \cdot 10^{-4}$	0.00	1.00	$3.00 \cdot 10^{-4}$	0.00	0.00	RCS
2	$10.00 \cdot 10^{-4}$	0.00	1.00	$1.00 \cdot 10^{-4}$	0.00	0.00	R(sonic)CS
3	$2.80 \cdot 10^{-4}$	−0.50	1.00	$2.80 \cdot 10^{-4}$	0.50	0.00	RCR
4	$2.90 \cdot 10^{-4}$	0.00	1.00	$2.40 \cdot 10^{-4}$	0.00	0.00	RCS
5	$2.34 \cdot 10^{-4}$	0.10	0.00	$2.74 \cdot 10^{-4}$	0.20	1.00	SCR
6	$1.90 \cdot 10^{-4}$	1.00	1.00	$2.20 \cdot 10^{-4}$	0.50	0.00	SCS

Table 2
Parameters used for Tests from 1 to 6: domain length ℓ, blood density ρ, vessel wall stiffness K, reference cross-sectional area A_0, external pressure p_e, location of the initial discontinuity x_d and output time t_{End}.

Test	Vessel	ℓ [m]	ρ	K[Pa]	A_0[m^2]	p_e[Pa]	x_d[m]	t_{End}[s]
1	Artery	0.50	1000.00	20 005.00	$3.14 \cdot 10^{-4}$	0.00	0.50ℓ	0.05
2	Artery	0.50	1000.00	20 005.00	$3.14 \cdot 10^{-4}$	0.00	0.50ℓ	0.04
3	Vein	0.50	1000.00	333.00	$3.14 \cdot 10^{-4}$	0.00	0.50ℓ	0.09
4	Vein	0.50	1000.00	333.00	$3.14 \cdot 10^{-4}$	0.00	0.50ℓ	0.10
5	Vein	0.50	1000.00	333.00	$3.14 \cdot 10^{-4}$	0.00	0.50ℓ	0.10
6	Vein	0.50	1000.00	333.00	$3.14 \cdot 10^{-4}$	0.00	0.30ℓ	0.15

1. (TV+TR) $\mathbf{Q}^*_{\text{PRESS},i+\frac{1}{2}} = \mathbf{Q}^*_{TR,i+\frac{1}{2}}$, with $\mathbf{Q}^*_{TR,i+\frac{1}{2}} = [A^*_{TR,i+\frac{1}{2}}, q^*_{TR,i+\frac{1}{2}}, 0]^T$ the (modified) approximate two rarefaction solution of the Riemann problem for the pressure system (70) in the Star Region presented in Section 5.1, for each cell i.
2. (TV+Lin.TR) $\mathbf{Q}^*_{\text{PRESS},i+\frac{1}{2}} = \mathbf{Q}^*_{LTR,i+\frac{1}{2}}$, with $\mathbf{Q}^*_{LTR,i+\frac{1}{2}} = [A^*_{LTR,i+\frac{1}{2}}, q^*_{LTR,i+\frac{1}{2}}, 0]^T$ the (modified) approximate linearized two rarefaction solution of the Riemann problem for the pressure system (70) in the Star Region presented in Section 5.2, for each cell i.

It is worth remarking that the third component of any solution just presented is set equal to 0 because the variable ϕ has no value due to the contact discontinuity λ_{p2} at the interface. In fact, there are two values ϕ^*_L and ϕ^*_R for each solution type, one to the left and one to the right of the interface, but we do not actually need them because the pressure flux in (22) has 0 as its third component.

7. Numerical results

In this section, we design test problems and assess the performance of the numerical splitting methods of type TV presented in this paper.

We propose six test problems; these tests have been chosen to represent the different admissible solutions of the 1D blood flow equations in the case of arteries (Tests 1 and 2) and veins (Tests 3, 4, 5, 6), namely smooth solutions (rarefactions), elastic jumps (shocks), and contact discontinuities. Of the three waves, the contact discontinuity is usually the one that presents a greater challenge, especially for linearized or incomplete solvers, since excessive numerical diffusion occurs in the form of smearing of the contact discontinuity. In the case of veins, the tests are constructed to explore different positions of A_c in (29) with respect to the tests data. This value is of critical importance for the wave pattern of the pressure system. As mentioned earlier, we will not address this issue in this paper, but we will restrict ourselves to showing that the presented schemes work properly even in cases when genuine non-linearity of the λ_{p1}- and λ_{p3}-characteristic fields of the pressure system is lost. The numerical results of the methods 1 and 2 are compared with the exact solution of the Riemann problem for the full 1D blood flow equations and some competing methods in literature. The initial data, expressed in terms of the physical variables A, u, and ϕ, can be found in Table 1. Meanwhile, the model parameters are provided in Table 2. The discussion of the numerical results is covered in Section 7.1, while an efficiency test is performed in Section 7.2.

7.1. Results discussion

Numerical results for both methods 1 and 2 are shown and plotted against the exact solution of the Riemann problem for the full 1D blood flow Eqs. (6) and the results of the Godunov method [43] used in conjunction with the exact Riemann solver for the complete 1D system (fully described in Toro [35]). For all tests, we use a Courant–Friedrichs–Lewy number $C_{cfl} = 0.9$ and a mesh of $I = 50$ computational cells (Figs. 3–8). In this work the Courant–Friedrichs–Lewy number C_{cfl} is defined as follows

Definition 7.1.

$$C_{cfl} = \frac{\Delta t}{\Delta x} S^n_{max}, \tag{73}$$

where

$$S^n_{max} = max_i \left\{ max_k \left| \lambda^n_{k,i} \right| \right\}, \quad k = 1, \dots, N, \quad i = 1, \dots, I; \tag{74}$$

where $\lambda^n_{k,i}$ is the k-th eigenvalue of the *complete system* (7) evaluated in cell i at time t^n, and N is the number of eigenvalues of the considered system.

Results from Test 1 (Artery). The solution of Test 1 consists of three waves, namely a left-facing rarefaction wave, a middle contact discontinuity, visible for the tracer ϕ, and a right-facing elastic jump, or shock (RCS). The left rarefaction wave carries smooth transitions of cross-sectional area A and velocity u, while the right shock carries discontinuous jumps in these quantities. The numerical results of the two new methods presented are comparable to those of the Godunov scheme: all approximations are accurate and very similar among themselves for the rarefaction wave, the contact and the shock wave, we can appreciate monotone shocks, i.e. there are no spurious oscillations in the vicinity of shocks and also the contact discontinuity presents a minimal smearing and its speed of propagation is correct.

Results from Test 2 (Artery). Test 2 contains the same wave pattern as Test 1, that is a left rarefaction, a middle contact and a right shock (RCS). However, there are two important differences. First, the strength of the waves; this may pose a challenge to the robustness of the methods. Second, the left rarefaction in Test 2 is transonic; i.e. the associated left eigenvalue $\lambda_1 = u - c$ transits monotonically from negative values to positive values, passing through a critical point at which $u = c$.

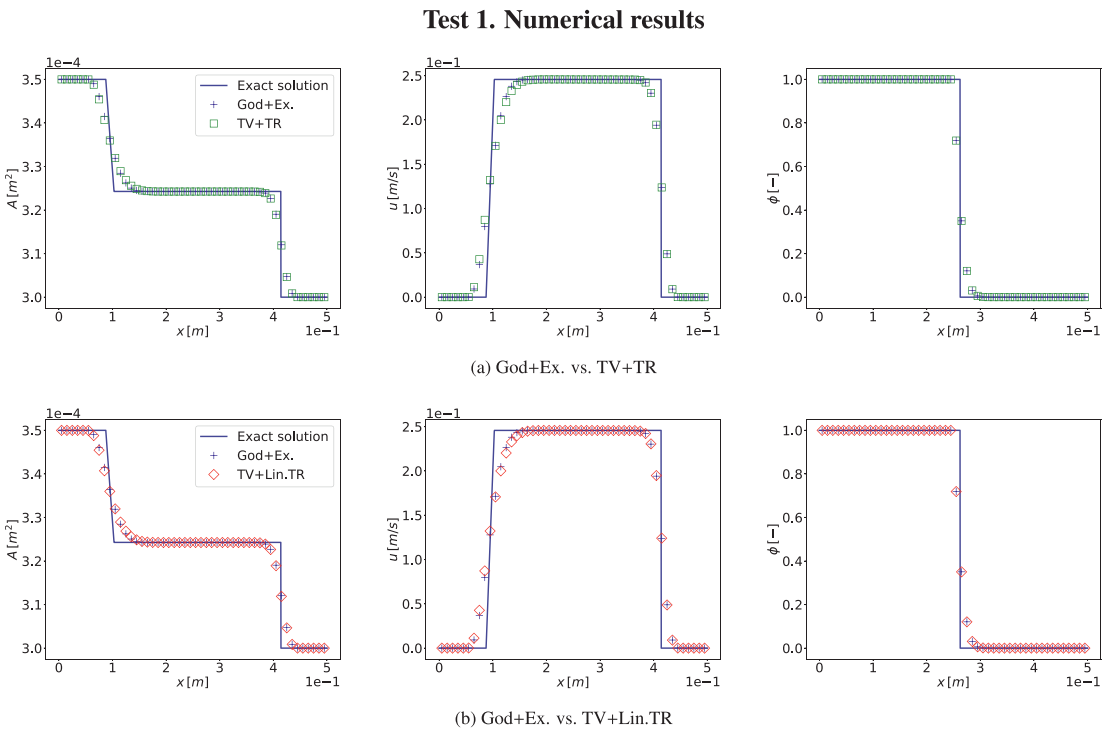

(a) God+Ex. vs. TV+TR

(b) God+Ex. vs. TV+Lin.TR

Fig. 3. Test 1. Artery. RCS. Numerical results of methods 1, 2 vs. the classic Godunov method with $C_{cfl} = 0.9$, $I = 50$ cells, and the exact solution of the Riemann problem for the complete system presented in [38,40]. Initial conditions and parameters are given in Tables 1 and 2.

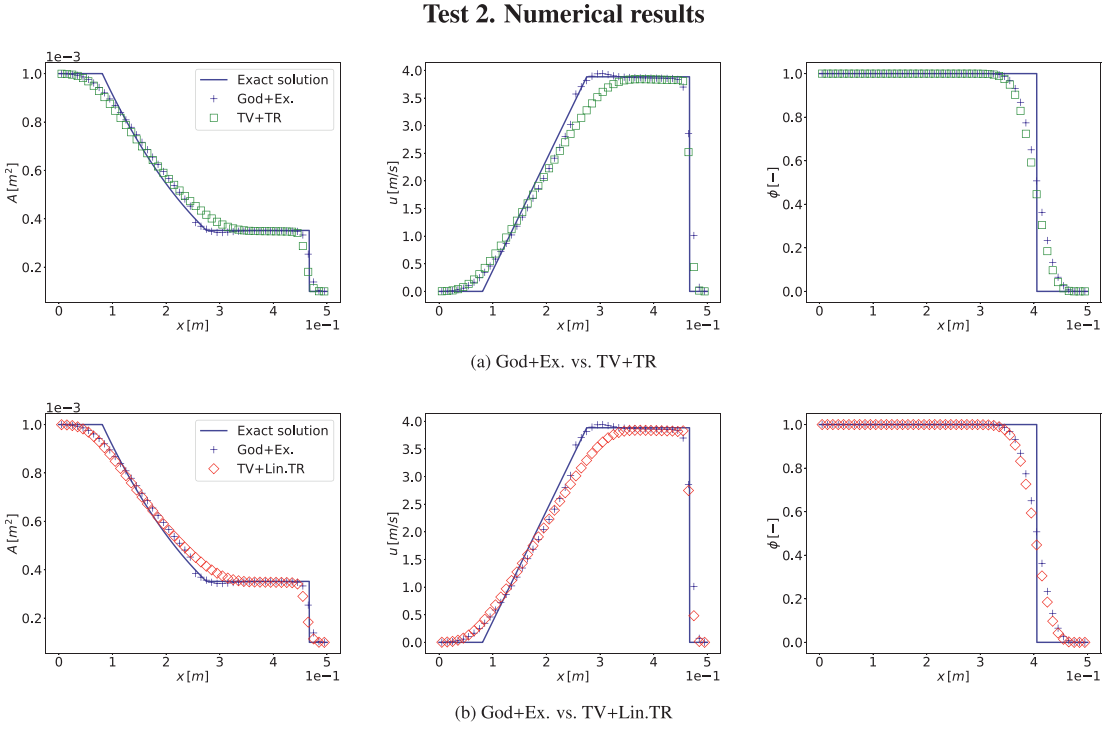

(a) God+Ex. vs. TV+TR

(b) God+Ex. vs. TV+Lin.TR

Fig. 4. Test 2. Artery. R(sonic)CS. Numerical results of methods 1, 2 vs. the classic Godunov method with $C_{cfl} = 0.9$, $I = 50$ cells, and the exact solution of the Riemann problem for the complete system presented in [38,40]. Initial conditions and parameters are given in Tables 1 and 2.

Even though the wave is smooth, the correct approximation of the sonic point is challenging for all numerical methods. Some schemes will present a jump (shock) instead of a smooth transition across the sonic point; this is sometimes referred to as the *entropy glitch* and arises only in the presence of sonic rarefaction waves. Such a shock is entropy violating and therefore unphysical. This problem was overcome by the two new schemes, which present smooth transitions for the area A and the velocity u. On the other hand, the results for both splitting schemes show a small overshoot for the velocity u in agreement with the shock front. The results for the contact discontinuity follow the path of the Godunov scheme and show a higher numerical diffusion. However, the propagation velocity and average position remain correct.

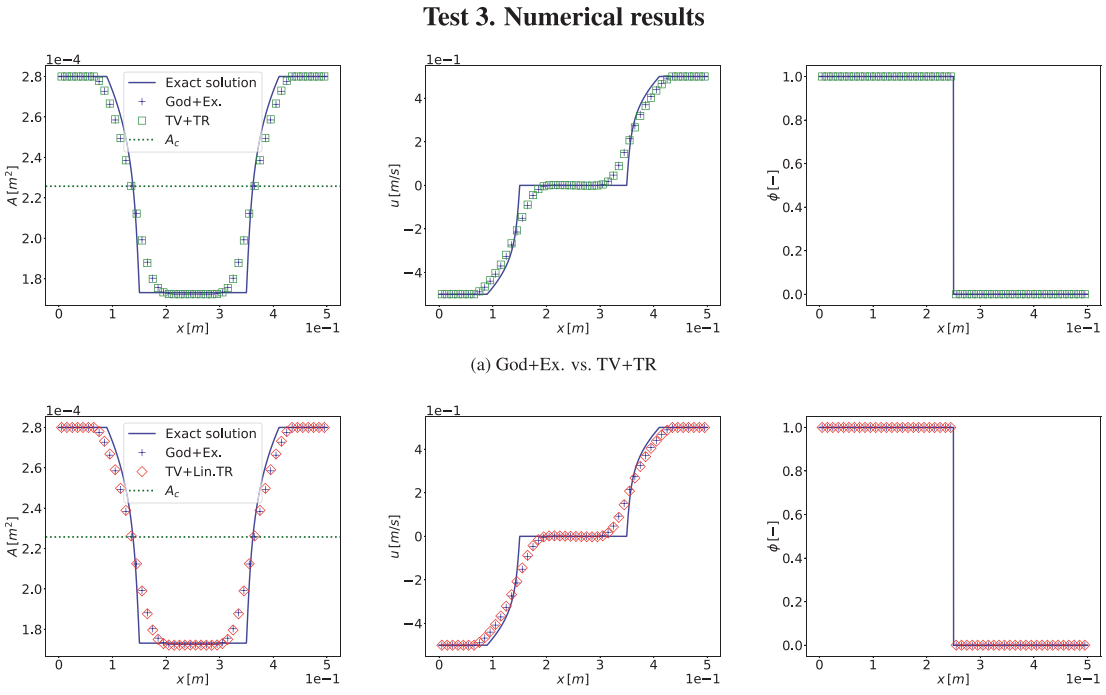

(a) God+Ex. vs. TV+TR

(b) God+Ex. vs. TV+Lin.TR

Fig. 5. Test 3. Vein. RCR. Numerical results of methods 1, 2 vs. the classic Godunov method with $C_{cfl} = 0.9$, $I = 50$ cells, and the exact solution of the Riemann problem for the complete system presented in [38,40]. Initial conditions and parameters are given in Tables 1 and 2. A_c in Eq. (29) is located inside both rarefactions.

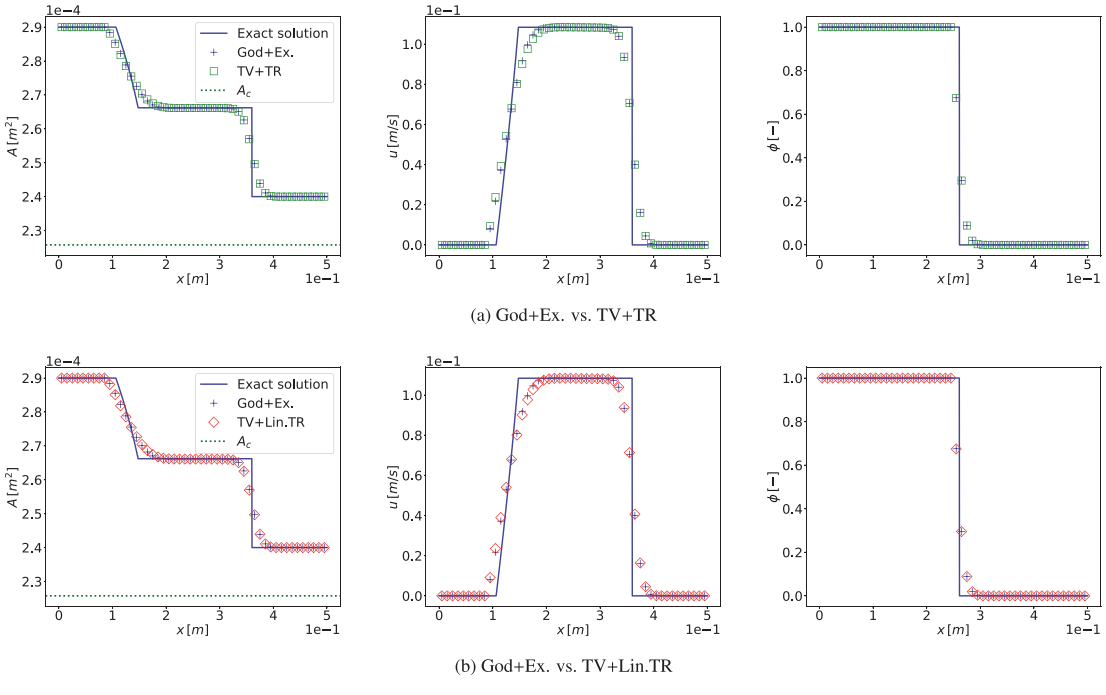

(a) God+Ex. vs. TV+TR

(b) God+Ex. vs. TV+Lin.TR

Fig. 6. Test 4. Vein. RCS. Numerical results of methods 1, 2 vs. the classic Godunov method with $C_{cfl} = 0.9$, $I = 50$ cells, and the exact solution of the Riemann problem for the complete system presented in [38,40]. Initial conditions and parameters are given in Tables 1 and 2. A_c in Eq. (29) is located below the range covered by the Riemann problem results.

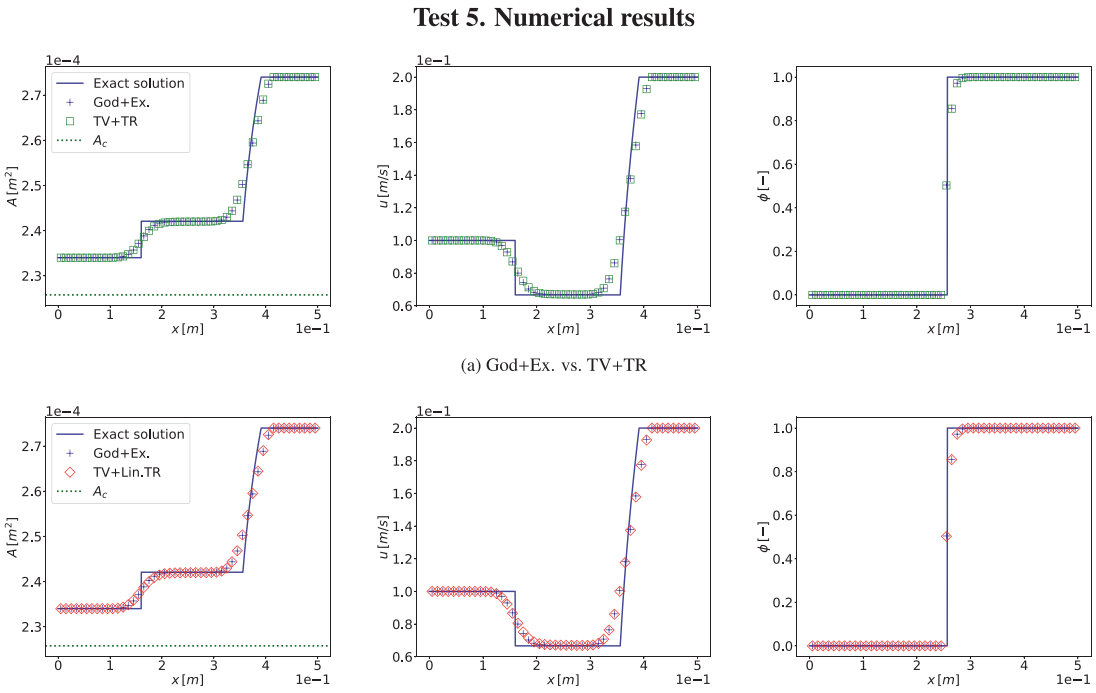

(a) God+Ex. vs. TV+TR

(b) God+Ex. vs. TV+Lin.TR

Fig. 7. Test 5. Vein. SCR. Numerical results of methods 1, 2 vs. the classic Godunov method with $C_{cfl} = 0.9$, $I = 50$ cells, and the exact solution of the Riemann problem for the complete system presented in [38,40]. Initial conditions and parameters are given in Tables 1 and 2. A_c in Eq. (29) is located below the range covered by the Riemann problem results.

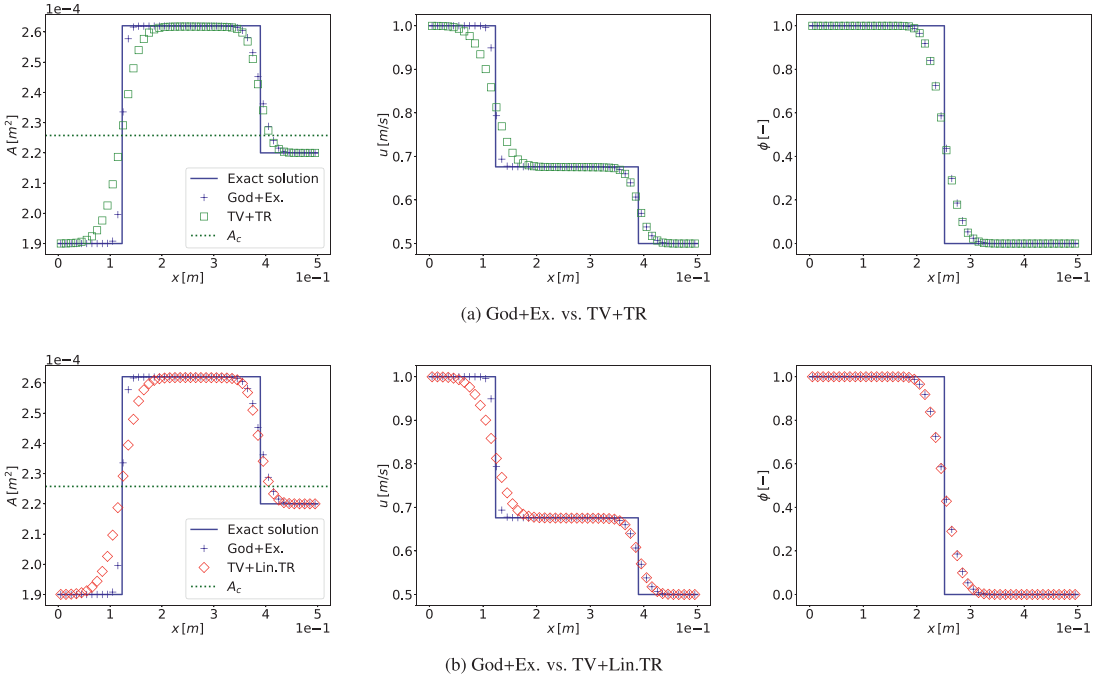

(a) God+Ex. vs. TV+TR

(b) God+Ex. vs. TV+Lin.TR

Fig. 8. Test 6. Vein. SCS. Numerical results of methods 1, 2 vs. the classic Godunov method with $C_{cfl} = 0.9$, $I = 50$ cells, and the exact solution of the Riemann problem for the complete system presented in [38,40]. Initial conditions and parameters are given in Tables 1 and 2. A_c in Eq. (29) is located inside both shocks.

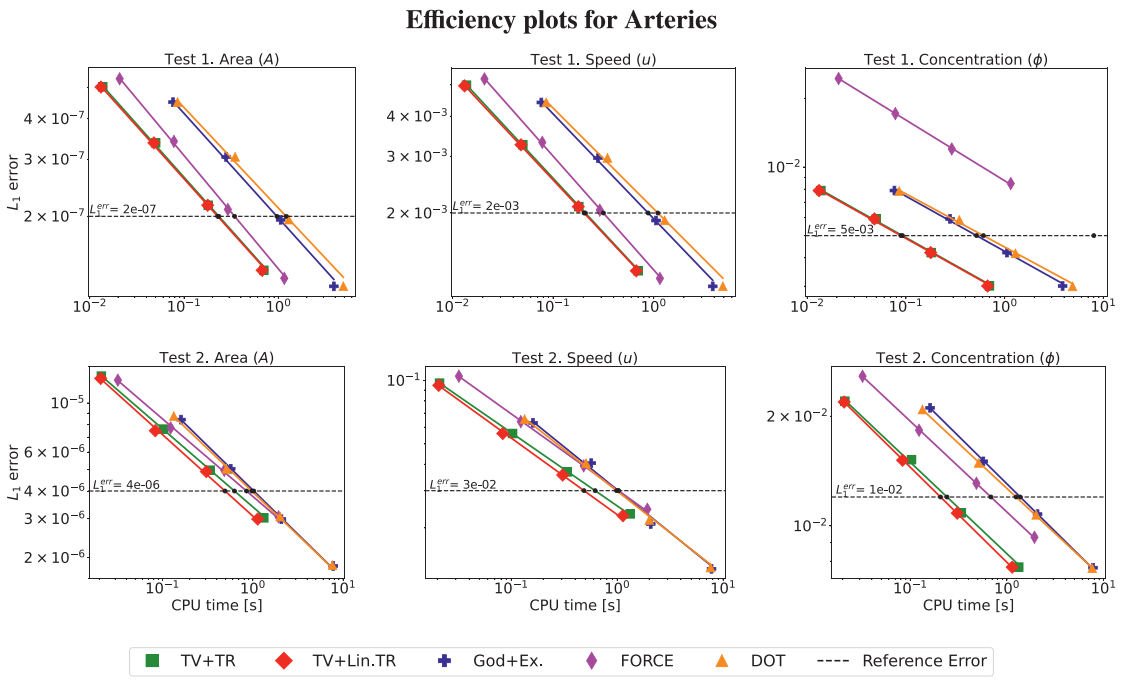

Fig. 9. Efficiency plots for Tests 1, 2, in Tables 1, 2, calculated for meshes $I = [50, 100, 200, 400]$. The lines represent the least square approximation (where possible) of the data.

Results from Test 3 (Vein). The solution of Test 3 consists of a left rarefaction, a middle contact discontinuity for ϕ and a right rarefaction (RCR), in this problem A_c is located *inside* the rarefactions; we can appreciate that the accuracy of the methods is not affected by this particular position of A_c, and the results of the new schemes are comparable with those of the Godunov method: in particular, the contact discontinuity is well described without smearing.

Results of Test 4 (Vein). The solution of Test 4 consists of a left rarefaction, a middle contact discontinuity, and a right shock (RCS), A_c is outside the range covered by the exact solution and its numerical approximations. The comments are similar to those of Test 3, with minimal diffusion in the approximation of the contact discontinuity.

Results from Test 5 (Vein). With the same position of A_c as in Test 4, this test scenario features a left shock, a middle contact discontinuity, and a right rarefaction (SCR) problem. Once again, the results obtained from the two new methods are comparable to those of the Godunov scheme. Notably, the left shock exhibits some smoothing in all of these schemes, while the contact discontinuity experiences minimal diffusion.

Results from Test 6 (Vein). Finally, the solution of Test 6 shows a left shock, a middle contact discontinuity, and a right shock (SCS) with A_c *inside* both shocks. While for the concentration of the passive scalar the results of the two new methods are comparable to those of the Godunov scheme, which describes the contact discontinuity with some diffusion, the left shock is smeared in the case of A and u, unlike in the Godunov scheme. We think that this difference could be due to the strength of the left shock and the non-linear behavior of the veins, and not to the particular position of A_c, because the latter is the same as that of the right shock.

7.2. Efficiency: Error against CPU time

Efficiency is determined by the CPU time required by a method to achieve a specified error E. To assess the efficiency of the TV-type methods presented in this study (methods 1 and 2), we compare the results with those obtained with standard and well known numerical methods. We consider two non-linear and complete solvers: the Godunov method with the exact Riemann solver (Section 7.1), the DOT Riemann solver [44,45] and a centered, and thus incomplete, scheme: the FORCE scheme [35,46]. Here we calculate the CPU cost and the L_1 error for each method cited above, for variables A, u and ϕ, with meshes $I = [50, 100, 200, 400]$ and a $C_{cfl} = 0.95$. L_1 error defined

$$L_1^{err}(t_{End}, \Delta x_j) = \Delta x_j \sum_{i=1}^{I_j} |q_{k,i}^{t_{End}} - q_{k,i}^{e}|, \quad k = 1, 2, 3; \tag{75}$$

being t_{End} the output time, $q_{k,i}^{t_{End}}$ the k-th component of $\mathbf{Q}_i^n$ at time t_{End}, $q_{k,i}^{e}$ the corresponding exact solution and $\Delta x_j = \ell / I_j$, with ℓ the vessel length and I_j the actual mesh. Results are depicted in Figs. 9, 10, 11.

In case of arteries, the two new methods prove to be the most efficient numerical methods (Figs. 9, 11). For the test in subsonic regime (Test 1) concerning the first two variables A and u, the new methods reach an accuracy comparable with that of the three classical numerical schemes (Godunov, FORCE, DOT) but with less computational effort. Regarding the concentration of the passive scalar, all methods reach the same level of accuracy with the exception of FORCE, due to its expected excessive numerical diffusion in the description of the intermediate wave (Fig. 9). In Test 2, where a left transonic rarefaction is depicted, the accuracy of the solution obtained with the new schemes is lower than the one of the solutions obtained with DOT and Godunov, regarding variables A and u (Fig. 9); however, the so-called *entropy glitch* must be taken into account. The two new methods in fact prove to reproduce this rarefaction in a smooth way.

As for veins, the method TV+Lin.TR proves to be the most efficient of the two new methods and for Tests 3, 4, 5 the most efficient of all the methods under analysis, achieving the same accuracy as the others, but in a lower CPU time. Also, the description of the concentration of the passive scalar ϕ is very accurate, a situation where instead FORCE usually fails, due to a high numerical diffusion (Figs. 10, 11). Test 6, on the other hand (left shock - middle contact - right shock in a vein), shows a remarkable decrease in accuracy for the two new methods, for variables A and u, with respect to the Godunov method and the DOT one, due to a higher diffusion in the description of the left shock (Fig. 10). In this case, the accuracy of the new methods is comparable to that of FORCE, on the contrary, the efficiency in describing the concentration ϕ is very good. In particular, the new methods exhibit a small diffusion in the description of ϕ, which, in contrast, is not present

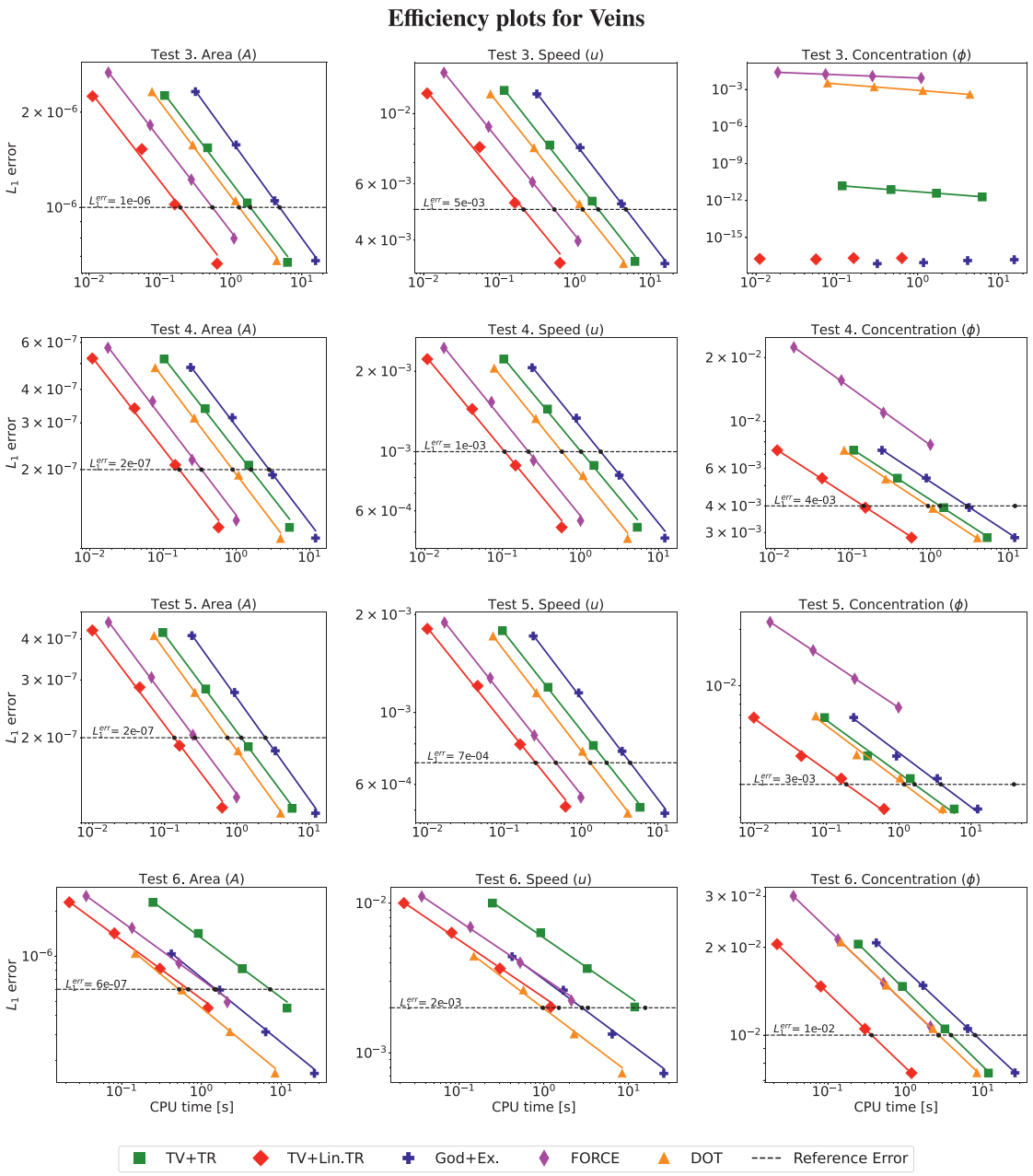

Fig. 10. Efficiency plots for Tests 3, 4, 5, 6 in Tables 1, 2, calculated for meshes $I = [50, 100, 200, 400]$. The lines represent the least square approximation (where possible) of the data.

in Test 3. For this reason, the concentration plot for this test is the result of round-off errors and the results in Fig. 11 are omitted.

It is worth noting that the FORCE scheme for the passive scalar ϕ generally does not achieve the chosen reference error with the given meshes, but the CPU time is calculated using an extrapolation of the observed convergence pattern. Furthermore, regarding both arteries and veins, we can conclude that the two TV methods here proposed proved to be as accurate as Godunov's scheme in describing the contact discontinuity.

8. Conclusions

In this work we have presented a flux splitting method at PDEs level for the original hyperbolic system of 1D blood flow equations with continuous parameters and an advection equation for a passive scalar, for both arteries and veins, separating the given system in advection system and pressure one. Consequently we have presented two approximated Riemann problem solvers for the obtained pressure system, and after, two final numerical flux splitting schemes for the complete 1D blood flow model have been built. These latter have been compared with the classic Godunov scheme and the exact solution of the Riemann problem for the complete system, in various test problems for arteries and veins, both in subsonic and transonic regime, proving that the issues faced with the lack of genuine non-linearity of two characteristic fields of the pressure system do not prevent the final splitting scheme from working properly. Finally an efficiency analysis has been carried out. The two proposed methods have proved to be in general considerably more efficient than the original Godunov method, the FORCE centered numerical scheme and the DOT Riemann solver, and can be considered as competitive methods to solve the Riemann problems under study. In the forthcoming research, the proposed techniques will be implemented to solve networks of 1D blood flow models.

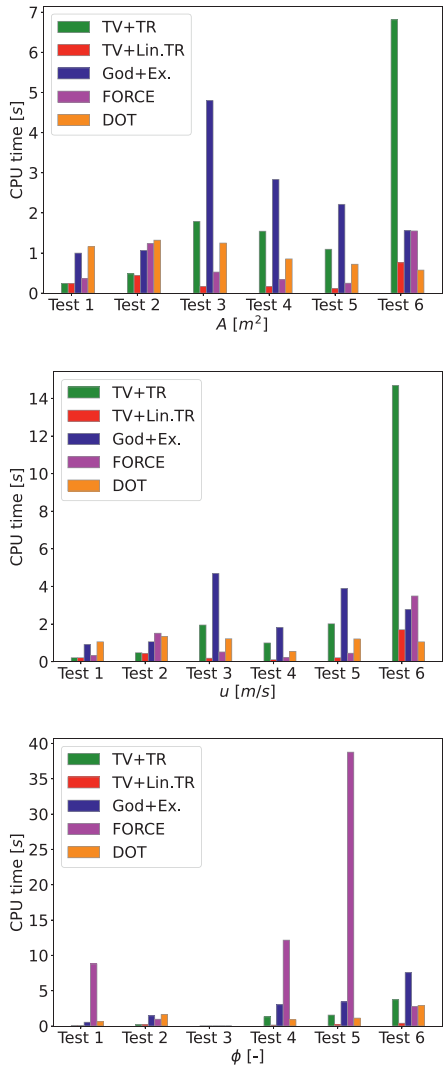

Fig. 11. Efficiency bar plots for Tests 1, 2, 3, 4, 5, 6 in Tables 1, 2 representing the actual time each method takes to reach errors given in Figs. 9, 10, for each variable.

Additionally, a comprehensive investigation of the complete solution of the Riemann problem for the pressure system will be conducted, with a focus on analyzing the implications of the loss of genuine non-linearity.

CRediT authorship contribution statement

Alessandra Spilimbergo: Conceptualization, Methodology, Software, Validation, Writing – original draft, Writing – review & editing. **Eleuterio F. Toro:** Conceptualization, Methodology, Software, Supervision, Validation, Writing – review & editing. **Annunziato Siviglia:** Conceptualization, Methodology, Supervision, Validation, Writing – review & editing. **Lucas O. Müller:** Conceptualization, Methodology, Software, Supervision, Validation, Writing – review & editing.

Declaration of competing interest

The authors declare that they have no known competing financial interests or personal relationships that could have appeared to influence the work reported in this paper.

Data availability

No data was used for the research described in the article.

Acknowledgments

Lucas O. Müller and Alessandra Spilimbergo are members of the *Gruppo Nazionale per il Calcolo Scientifico dell' Istituto Nazionale di Alta Matematica* (INdAM-GNCS, Italy). Alessandra Spilimbergo acknowledges the University of Trento, Italy for financing her Ph.D. studentship.

Appendix. Newton–Raphson method

Here we present the Newton–Raphson method used to solve (58). The others are similar in structure, with the same tolerances. This method is written in the Python language.

```
# ################################################
# Newton–Raphson method
# ################################################

#initial value for As:
As=AL
for i in range(50):
  #functTR is described in (58)
  #c is the wave speed (9)
  fun=self.functTR(As, AL, qS, qL)
  df=self.c(As)
  alpha = 1.
  for i2 in range(50):
    aAux = As - alpha*fun/df
    if aAux > 0.:
      fAux=self.functTR(aAux, AL, qS, qL)
      if np.abs(fAux) <= np.abs(fun):
        break
      else:
        alpha *= 0.8
    else:
      alpha *= 0.8
  AsOld=As
  As = As - alpha*fun/df
  if np.abs(np.abs(As-AsOld)/((As+AsOld)/2.))<1e-7:
    break
  if i==(50-1):
    print('No_convergence')
    exit(-1)
return[As,qS]
```

References

[1] Bazilevs Y, Calo V, Zhang Y, Hughes T. Isogeometric fluid–structure interaction analysis with applications to arterial blood flow. Comput Mech 2006;38:310–22. http://dx.doi.org/10.1007/s00466-006-0084-3.

[2] Crosetto P, Reymond P, Deparis S, Kontaxakis D, Stergiopulos N, Quarteroni A. Fluid–structure interaction simulation of aortic blood flow. Comput & Fluids 2011;43(1):46–57. http://dx.doi.org/10.1016/j.compfluid.2010.11.032.

[3] Hughes T, Lubliner J. On the one-dimensional theory of blood flow in the larger vessels. Math Biosci 1973;18:161–70. http://dx.doi.org/10.1016/0025-5564(73)90027-8.

[4] Formaggia L, Lamponi D, Quarteroni A. One-dimensional models for blood flow in arteries. J Engrg Math 2003;47:251–76. http://dx.doi.org/10.1023/B:ENGI.0000007980.01347.29.

[5] Sherwin S, Franke V, Peiró J, Parker K. One-dimensional modelling of a vascular network in space-time variables. J Engrg Math 2003;47:217–50. http://dx.doi.org/10.1023/B:ENGI.0000007979.32871.e2.

[6] Mynard J, Nithiarasu P. A 1D arterial blood flow model incorporating ventricular pressure, aortic valve and regional coronary flow using the locally conservative Galerkin (LCG) method. Commun Numer Methods Eng 2008;24(5):367–417. http://dx.doi.org/10.1002/cnm.1117.

[7] Müller L, Toro E. A global multi-scale model for the human circulation with emphasis on the venous system. Int J Numer Methods Biomed Eng 2014;30(7):681–725. http://dx.doi.org/10.1002/cnm.2622.

[8] Müller L, Toro E. Enhanced global mathematical model for studying cerebral venous blood flow. J Biomech 2014;47(13):3361–72. http://dx.doi.org/10.1016/j.jbiomech.2014.08.005.

[9] Grinberg L, Cheever E, Anor T, Madsen J, Karniadakis G. Modeling blood flow circulation in intracranial arterial networks: A comparative 3D/1D simulation study. Ann Biomed Eng 2011;39:297–309. http://dx.doi.org/10.1007/s10439-010-0132-1.

[10] Xiao N, Alastruey J, Figueroa A. A systematic comparison between 1-D and 3-D hemodynamics in compliant arterial models. Int J Numer Methods Biomed Eng 2014;30(2):204–31. http://dx.doi.org/10.1002/cnm.2598.

[11] Boileau E, Nithiarasu P, Blanco P, Müller L, Fossan F, Hellevik L, et al. A benchmark study of numerical schemes for one-dimensional arterial blood flow modelling. Int J Numer Methods Biomed Eng 2015;31(10). http://dx.doi.org/10.1002/cnm.2732.

[12] Matthys K, Alastruey J, Peiró J, Khir A, Segers P, Verdonck P, et al. Pulse wave propagation in a model human arterial network: Assessment of 1D numerical simulations against in vitro measurements. J Biomech 2007;40(15):3476–86. http://dx.doi.org/10.1016/j.jbiomech.2007.05.027.

[13] Bessems D, Giannopapa C, Rutten M, van de Vosse F. Experimental validation of a time-domain-based wave propagation model of blood flow in viscoelastic vessels. J Biomech 2008;41(2):284–91. http://dx.doi.org/10.1016/j.jbiomech.2007.09.014.

[14] Olufsen M, Peskin C, Kim W, Pedersen E, Nadim A, Larsen J. Numerical simulation and experimental validation of blood flow in arteries with structured-tree outflow conditions. Ann Biomed Eng 2000;28:1281–99. http://dx.doi.org/10.1114/1.1326031.

[15] Reymond P, Merenda F, Perren F, Rüfenacht D, Stergiopulos N. Validation of a one-dimensional model of the systemic arterial tree. Am J Physiol Heart Circ Physiol 2009;297(1):H208–22. http://dx.doi.org/10.1152/ajpheart.00037.2009.

[16] Liang F, Takagi S, Himeno R, Liu H. Biomechanical characterization of ventricular–arterial coupling during aging: A multi-scale model study. J Biomech 2009;42(6):692–704. http://dx.doi.org/10.1016/j.jbiomech.2009.01.010.

[17] Mynard J, Smolich J. One-dimensional haemodynamic modeling and wave dynamics in the entire adult circulation. Ann Biomed Eng 2015;43:1443–60. http://dx.doi.org/10.1007/s10439-015-1313-8.

[18] Blanco P, Watanabe S, Passos M, Lemos P, Feijóo R. An anatomically detailed arterial network model for one-dimensional computational hemodynamics. IEEE Trans Biomed Eng 2015;62(2):736–53. http://dx.doi.org/10.1109/TBME.2014.2364522.

[19] Formaggia L, Quarteroni A, Vergara C. On the physical consistency between three-dimensional and one-dimensional models in haemodynamics. J Comput Phys 2013;244:97–112. http://dx.doi.org/10.1016/j.jcp.2012.08.001.

[20] Blanco P, Feijóo R. A dimensionally-heterogeneous closed-loop model for the cardiovascular system and its applications. Med Eng Phys 2013;35(5):652–67. http://dx.doi.org/10.1016/j.medengphy.2012.07.011.

[21] Quarteroni A, Manzoni A, Vergara C. The cardiovascular system: Mathematical modelling, numerical algorithms and clinical applications. Acta Numer 2017;26:365–590. http://dx.doi.org/10.1017/S0962492917000046.

[22] Hellevik L, Vierendeels J, Kiserud T, Stergiopulos N, Irgens F, Dick E, et al. An assessment of ductus venosus tapering and wave transmission from the fetal heart. Biomech Model Mechanobiol 2009;8:509–17. http://dx.doi.org/10.1007/s10237-009-0155-4.

[23] Brook B, Falle S, Pedley T. Numerical solutions for unsteady gravity-driven flows in collapsible tubes: evolution and roll-wave instability of a steady state. J Fluid Mech 1999;396:223–56. http://dx.doi.org/10.1017/S0022112099006084.

[24] Sherwin S, Formaggia L, Peiró J, Franke V. Computational modelling of 1D blood flow with variable mechanical properties and its application to the simulation of wave propagation in the human arterial system. Internat J Numer Methods Fluids 2003;43(6–7):673–700. http://dx.doi.org/10.1002/fld.543.

[25] Ghitti B, Berthon C, Le M, Toro E. A fully well-balanced scheme for the 1D blood flow equations with friction source term. J Comput Phys 2020;421:109750. http://dx.doi.org/10.1016/j.jcp.2020.109750.

[26] Pimentel-García E, Müller L, Toro E, Parés C. High-order fully well-balanced numerical methods for one-dimensional blood flow with discontinuous properties. J Comput Phys 2023;475:111869. http://dx.doi.org/10.1016/j.jcp.2022.111869.

[27] Steger J, Warming R. Flux vector splitting of the inviscid gasdynamic equations with application to finite-difference methods. J Comput Phys 1981;40(2):263–93. http://dx.doi.org/10.1016/0021-9991(81)90210-2.

[28] van Leer B. Flux vector splitting for the Euler equations. Technical report, 1982.

[29] Liou M, Steffen C. A new flux splitting scheme. J Comput Phys 1993;107(1):23–39. http://dx.doi.org/10.1006/jcph.1993.1122.

[30] Zha G, Bilgen E. Numerical solutions of Euler equations by using a new flux vector splitting scheme. Internat J Numer Methods Fluids 1993;17(2):115–44. http://dx.doi.org/10.1002/fld.1650170203.

[31] Toro E, Vázquez-Cendón M. Flux splitting schemes for the Euler equations. Comput & Fluids 2012;70:1–12. http://dx.doi.org/10.1016/j.compfluid.2012.08.023.

[32] Toro E, Siviglia A, Spilimbergo A, Müller L. Advection-pressure splitting schemes for the equations of blood flow. Conservative and non-conservative forms. East Asian J Appl Math 2024 [in press].

[33] Leveque R. Numerical methods for conservation laws. Birkhäuser Verlag; 1999, http://dx.doi.org/10.1007/978-3-0348-5116-9.

[34] Godlewski E, Raviart P. Numerical approximation of hyperbolic systems of conservation laws. Springer; 1996, http://dx.doi.org/10.1007/978-1-4612-0713-9.

[35] Toro E. Riemann solvers and numerical methods for fluid dynamics: a practical introduction. 3rd ed.. Springer-Verlag Berlin Heidelberg; 2009, http://dx.doi.org/10.1007/b79761.

[36] Siviglia A, Toffolon M. Steady analysis of transcritical flows in collapsible tubes with discontinuous mechanical properties: implications for arteries and veins. J Fluid Mech 2013;736:195–215. http://dx.doi.org/10.1017/jfm.2013.542.

[37] Spilimbergo A, Toro E, Müller L. Exact solution of the Riemann problem for the one-dimensional blood flow equations with general momentum correction coefficient. Commun Comput Phys 2024 [in revision].

[38] Toro E, Siviglia A. Flow in collapsible tubes with discontinuous mechanical properties: mathematical model and exact solutions. Commun Comput Phys 2013;13(2):361–85. http://dx.doi.org/10.4208/cicp.210611.240212a.

[39] Smoller J. Shock waves and reaction-diffusion equations. 2nd ed.. Springer New York, NY; 1994, http://dx.doi.org/10.1007/978-1-4612-0873-0.

[40] Spilimbergo A, Toro E, Müller L. One-dimensional blood flow with discontinuous properties and transport: Mathematical analysis and numerical schemes. Commun Comput Phys 2021;29(03):649–97. http://dx.doi.org/10.4208/cicp.OA-2020-0132.

[41] Liu T. The Riemann problem for general 2 × 2 conservation laws. Trans Amer Math Soc 1974;199:89–112. http://dx.doi.org/10.2307/1996875.

[42] Toro E, Castro C, Vanzo D, Siviglia A. A flux-vector splitting scheme for the shallow water equations extended to high-order on unstructured meshes. Internat J Numer Methods Fluids 2022;1–27. http://dx.doi.org/10.1002/fld.5099.

[43] Godunov S. Finite difference method for numerical computation of discontinuous solutions of the equations of fluid dynamics. Mat Sb 1959;47:271–306.

[44] Dumbser M, Toro E. A simple extension of the Osher Riemann solver to non-conservative hyperbolic systems. J Sci Comput 2011;48:70–88. http://dx.doi.org/10.1007/s10915-010-9400-3.

[45] Dumbser M, Toro E. On universal Osher-type schemes for general nonlinear hyperbolic conservation laws. Commun Comput Phys 2011;10(3):635–71. http://dx.doi.org/10.4208/cicp.170610.021210a.

[46] Toro E, Billett S. Centred TVD schemes for hyperbolic conservation laws. IMA J Numer Anal 2000;20(1):47–79. http://dx.doi.org/10.1093/imanum/20.1.47.